Supplementary file

Material and Methods

The sorption of phosphorus onto iron oxides was evaluated by adding 0.2 mM ferrous iron (as $FeCl_2$) to 50 mL of 0.56 M NaCl or seawater (low-nutrient Sargasso seawater, LNSS, from OSIL®) containing phosphate (ranging from 0-70 µM) and silica (at concentrations of 0, 0.67, and 2.2 mM). To evaluate the influence of Ca^{2+} and Mg^{2+}, a solution of 0.56 M NaCl was amended to 10 mM Ca^{2+} and 50 mM Mg^{2+} in order to approximate the modern ocean concentrations, and up to 50 mM Ca^{2+} and 45 mM Mg^{2+} to mimic the Precambrian oceans. A stock 1000 ppm Si solution (Merck, 03793) was used to achieve the desired silica concentrations, a 1000 ppm phosphate stock was prepared from reagent grade KH_2PO_4, and calcium and magnesium additions were made from 1.0 M stock solutions. All co-precipitation experiments were conducted in acid washed (10% HCl) 100 ml plastic beakers at room temperature and pH was continuously monitored. A pH of 8.0 (± 0.1) was maintained throughout all experiments by the dropwise addition of dilute HCl or NaOH. Atmospheric O_2 was supplied by vigorous stirring. After the addition of ferrous iron, each experiment was allowed to react for 30 minutes to ensure complete iron oxidation, which was verified using the ferrozine assay. After the 30-minute reaction period, samples were filtered through 0.22 µm pore size, nylon syringe filters, and phosphate concentrations in the supernatant were measured spectrophotometrically. To test for phosphate removal due to mineral precipitation or sorption in the absence of iron, various concentrations of Si (0, 0.67, 2.2 mM) and high concentrations of phosphate (26-30 µM) were added to seawater in 50 mL centrifuge tubes at pH 8.0. A sub-sample was filtered immediately, and the tubes were then shaken for 20 hours and sampled again. No difference in dissolved P concentrations was measured over the 20-hour period. All phosphate concentrations were measured spectrophotometrically by the ascorbic acid method as described previously (Grasshoff et al., 1999). No silica interferences were observed. Distribution coefficients (K_Ds) were calculated from the slope of a linear regression generated by selecting the consecutive data points from the origin that gave the highest R^2.

From the phosphorus sorption experiments' calculated K_Ds at Si=0, 0.67, and 2.2 mM, interpolation surfaces were fitted to the results. It was found that measured K_Ds at other silica concentrations can be reasonably calculated by scaling the surface K_D interpolant at 0.67 mM Si such that for Si ≥ 0.67 mM, $K_D(Mg,Ca,Si) = K_D(Mg,Ca,0.67)\times(1+(Si-0.67)\times\alpha_2)$, where $\alpha_2=(0.008/0.042-1)/(2.2-0.67)$, and where elements Mg, Ca, and Si represent concentrations in mM. For Si < 0.67 mM, we use $K_D(Mg,Ca,Si) = K_D(Mg,Ca,0.67)\times(0.29/0.042+(Si\times\alpha_1))$, where $\alpha_1=(1-0.29/0.042)/(0.67-0)$. As can be seen from Fig. DR1, this approach gives reasonable results for most of the experimental data, except the K_D value for NaCl with Si=0 mM, Ca=10 mM, and Mg=50 mM. We view this latter experimental result as an experimental outlier as it does not follow the tendencies of the other data.

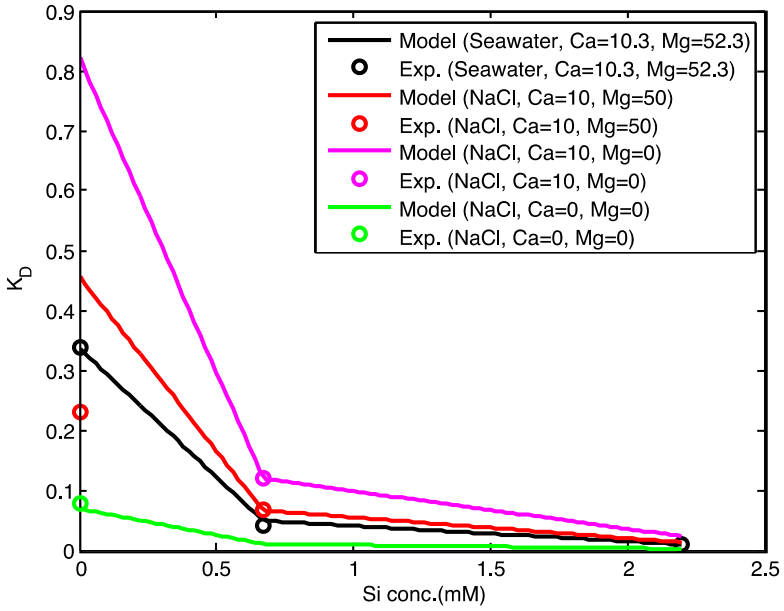

Figure DR1. Comparison of model interpolation to experimental K_D, using the equations above. Note that one experimental point is not reproduced by the model interpolation.

Modeling Details and Sensitivity Tests

We estimate the Mg^{2+} and Ca^{2+} concentrations of the Precambrian ocean following the method of Hardie (Hardie, 2003), which quantifies the flux of Mg^{2+} and Ca^{2+} from hydrothermal fluids and riverine sources. We assess the flux of hydrothermal fluids using the model of Sleep and Zahnle (Sleep and Zahnle, 2001) as implemented by Bjerrum and Canfield (Bjerrum and Canfield, 2004). In this model, the mid-ocean ridge hydrothermal flux is proportional to mid-ocean ridge spreading rates, in turn linked to mantle heat flux that decreases from 4x present day level through Earth history (Sleep and Zahnle, 2001),. In our model, we assume that the riverine flux is proportional to continental volume and silicate weathering, which is dependent on global mean temperature, where it is assumed that the faint young sun was always compensated to give clement conditions on Earth. Further, we assume continental volume increases beginning in the early Archean, following the results of Kamber et al. (Kamber et al., 2003), with a peak growth rate around 2.7 Ga (Condie et al., 2009). Based on these assumptions, we find that the long term ratio of hydrothermal mid ocean ridge/ river water (MOR/RW flux ratio) would have decreased exponentially over time (Figure DR2). From the MOR/RW flux ratio, we can calculate the long term evolution of Mg^{2+} and Ca^{2+} concentrations in the ocean following the approach of Hardie (2003).

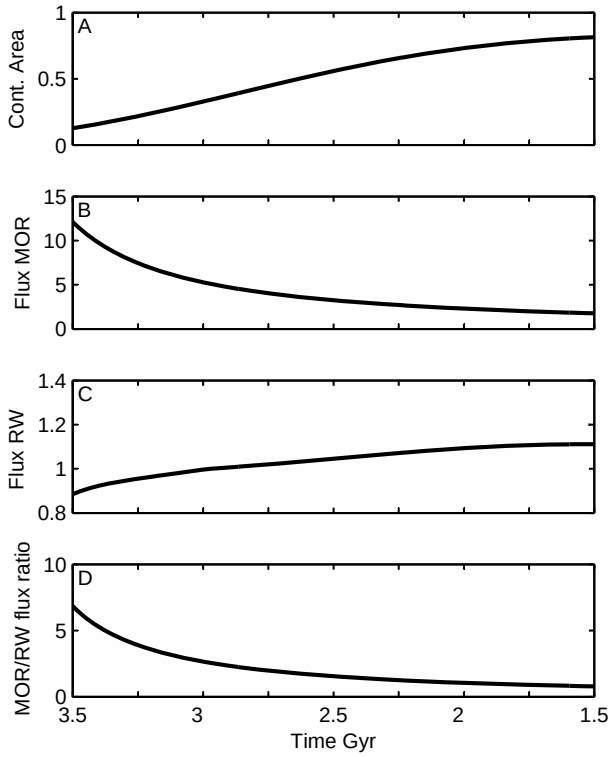

Figure DR2. Modelled long term evolution of fluxes. A) Continental growth from (Kamber et al., 2003). B) Model normalized mid ocean ridge (MOR) hydrothermal flux. C) Model normalized river water (RW) flux. D) MOR/RW flux ratio normalized to the present day ratio. Note that the normalized river (RW) flux is assumed to depend on both the continental growth and the CO_2 climate-driven weathering rate.

However, as stated in the main text, plate spreading rates and associated hydrothermal activity could have varied over intermediate timescales, resulting in second order variation with periodically higher Mg^{2+} concentrations (Hardie, 2003). Hardie used granite-pluton production in North America as a proxy to calculate the hydrothermal mid ocean ridge/ river water (MOR/RW) flux ratio, as he argued that granite plutonism and ocean-crust production are coupled crust forming processes operating at opposite ends of a moving plate. We incorporate Hardie's secular variation by subtracting the long term mean from his MOR/RW flux ratio and adding this to our MOR/RW flux ratio normalized to the present day ratio (Fig. DR3E). Based on the modeled Mg^{2+} and Ca^{2+} concentrations, we used the K_D interpolation routine described above to calculate the appropriate P_d from the observed P/Fe in BIFs (Figs. DR3B, C, and D, and Table DR1).

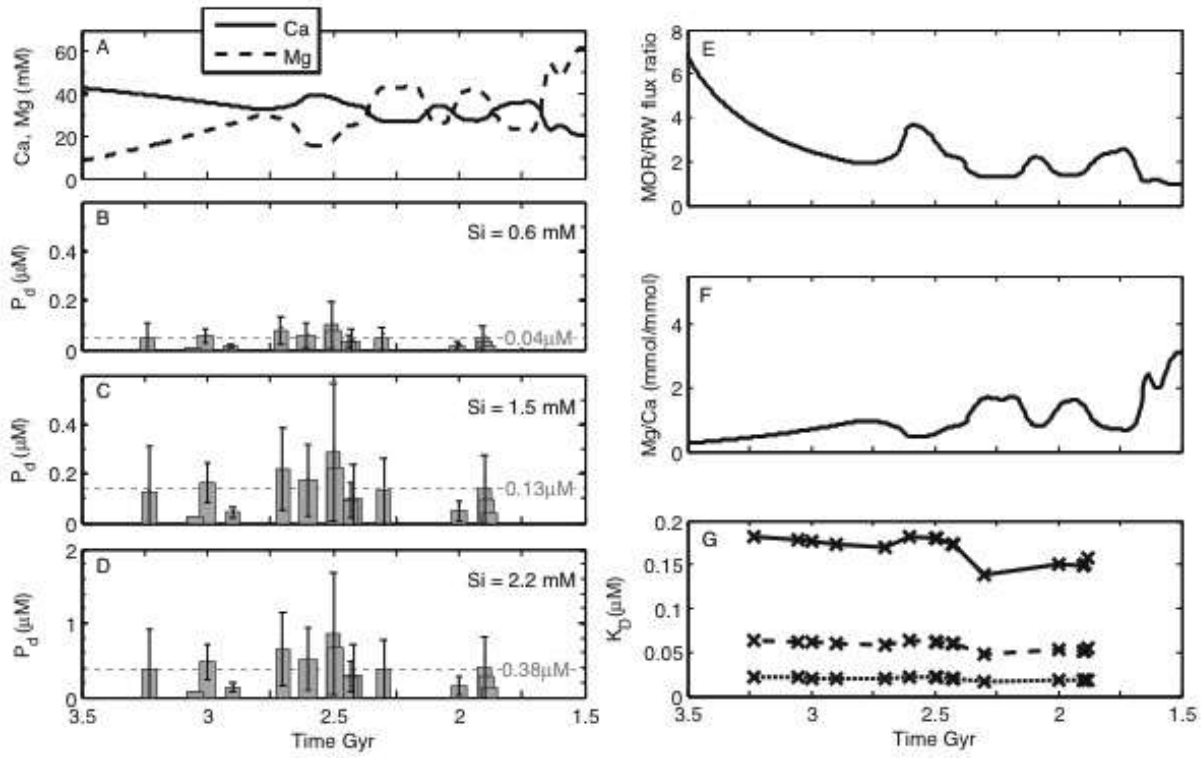

Figure DR3: The base case of our model. Panels in the left column are the same as Figure 3 in the main text, showing modeled Archean-Proterozoic ocean concentrations of Mg^{2+} and Ca^{2+} and calculated ocean phosphorus concentrations based on observed P/Fe^{3+} ratios of BIFs and experimentally determined distribution coefficients at three silica concentrations interpolated as a function of the modeled Mg^{2+} and Ca^{2+} concentrations. A grey dashed line indicates the mean value at each silica concentration. In the right column: E) Long term mid-ocean ridge/river-water flux ratios (MOR/RW) evolution combined with Hardie's (2003) secular variation; F) Mg/Ca derived from the mixing model of Hardie (2003) using the MOR/RW evolution model; G) Distribution coefficient (K_D) of P adsorption on iron oxides, derived from the interpolation surface of experimental results and calculated Mg and Ca concentrations through time for Si=0.6 mM (solid line), Si=1.5 mM (dashed line), and Si=2.2 mM (stippled line). X's mark times of BIF occurrences.

Recently, it has been proposed that the thermal evolution of the mantle of the early earth was quite different from previous understanding ((Korenaga, 2011) versus references in (Sleep and Zahnle, 2001)). Korenaga (2011) modeled thermal evolution and plate tectonics using a new scaling of plate tectonic convection based on fully dynamic calculations. In contrast to our base model, he finds that the heat flux and spreading rate was lower than the Cenozoic throughout the Late Archean and Proterozoic (Figure DR4). We tested implications of Korenaga's heat flux and spreading rate by implementing these into our model as seen in Figure DR5. We find that the much reduced heat flux and spreading rate only increases the Mg^{2+} and decreases the Ca^{2+} a little relative to our base case, resulting in little change of the calculated P_d. This may seem counter intuitive, but it has a relatively simple explanation. As spreading rate is low, there is a reduced MOR flux (with Mg^{2+}-Ca^{2+} exchange). Lower spreading rate also means less CO_2 degassing, lower CO_2 in the atmosphere, and a cooler climate, resulting in reduced continental weathering and a reduced river flux, accentuated by the smaller continental volume at the time. Overall for

the Archean-Paleoproterozoic, there is only a small reduction in the MOR/River flux ratio for reduced spreading rate, giving only a small increase in the Mg^{2+}/ Ca^{2+} ratio.

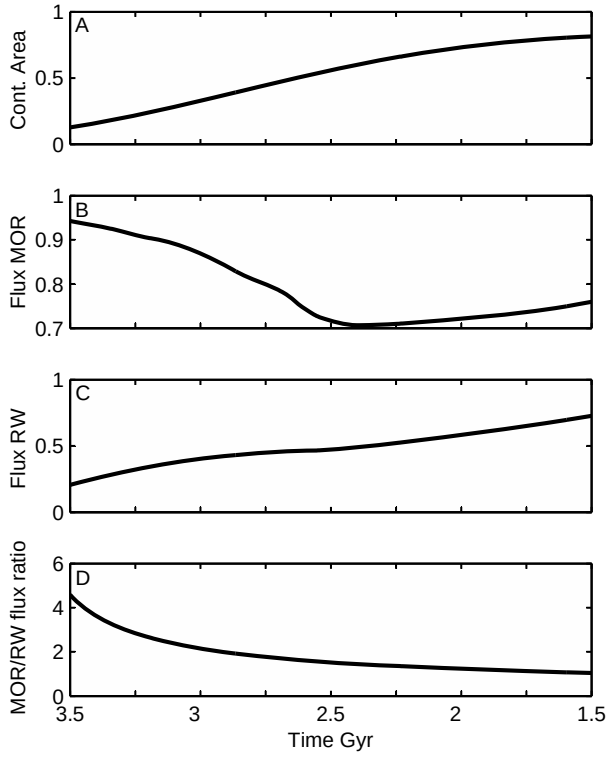

Figure DR4: Modelled long term evolution of fluxes based on Korenaga et al. (2011). Labels are as in Figure DR2.

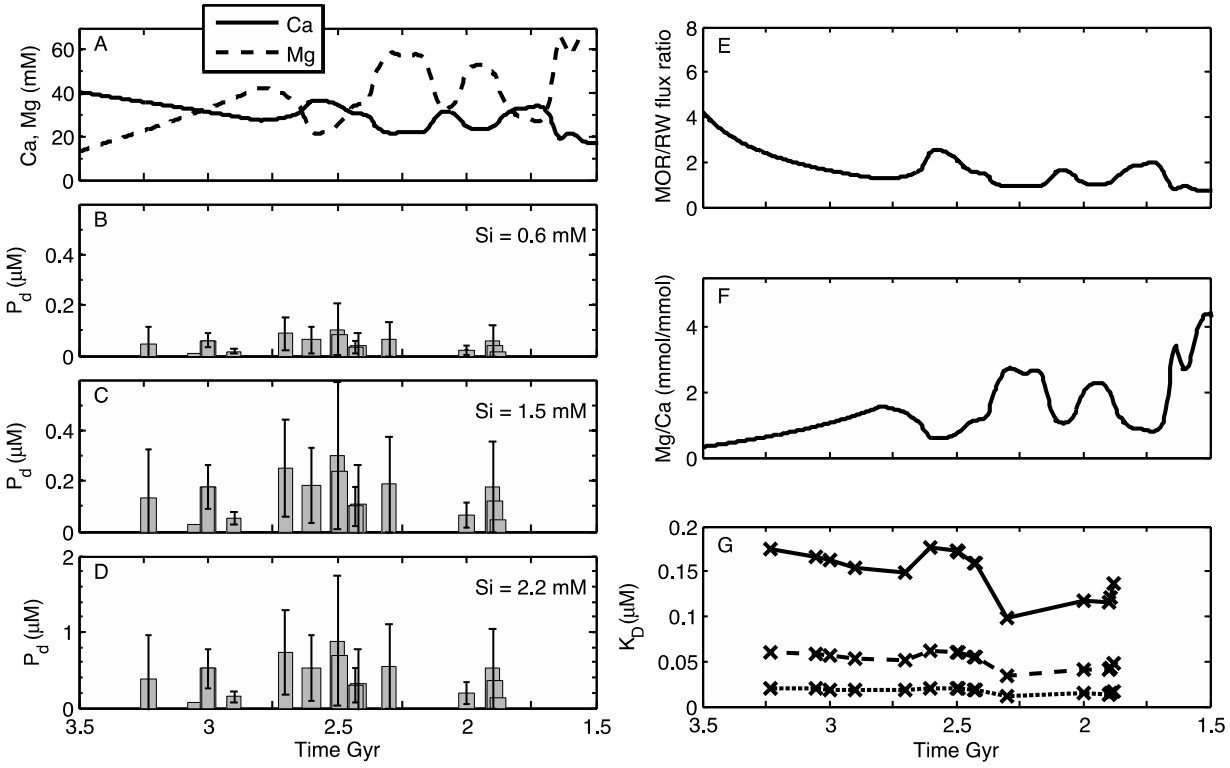

Figure DR5: The Korenaga case of our model. Labels are as in Figure DR3.

There are some uncertainties in the parameters used in modeling the evolution of Mg^{2+} and Ca^{2+} concentrations. First, in simplifying, we have followed Hardie (2003) in assuming that the oceanic Ca cycle is at steady state and saturated with respect to $CaCO_3$. We posit that the ocean Ca cycle over long timescales is likely in a dynamic steady state, while it may not be in dynamic steady state on a shorter timescale, as in the latter part of the Cenozoic (Fantle and DePaolo, 2005). However, to assess the uncertainties, we make a series of sensitivity tests of the possible implications of Mg^{2+} and Ca^{2+} concentrations different than those arrived at in the base model. As one set of end member conditions, we impose constant Mg^{2+} and Ca^{2+} concentrations the same as seawater today, 52.8 mM Mg^{2+} and 10.3 mM Ca^{2+} (Figure DR6). This results in increased P_d relative to the base model, ranging from an average of 0.14 to 0.76 µM for the two extreme silica concentrations. Imposing Mg^{2+} and Ca^{2+} concentrations as thought to have occurred in the Cretaceous, 42.5 mM Ca^{2+} and Mg^{2+} (Figure DR7), results in little change in P_d relative to the base model (both having an average of 0.04 to 0.38 µM for the two extreme silica concentrations).

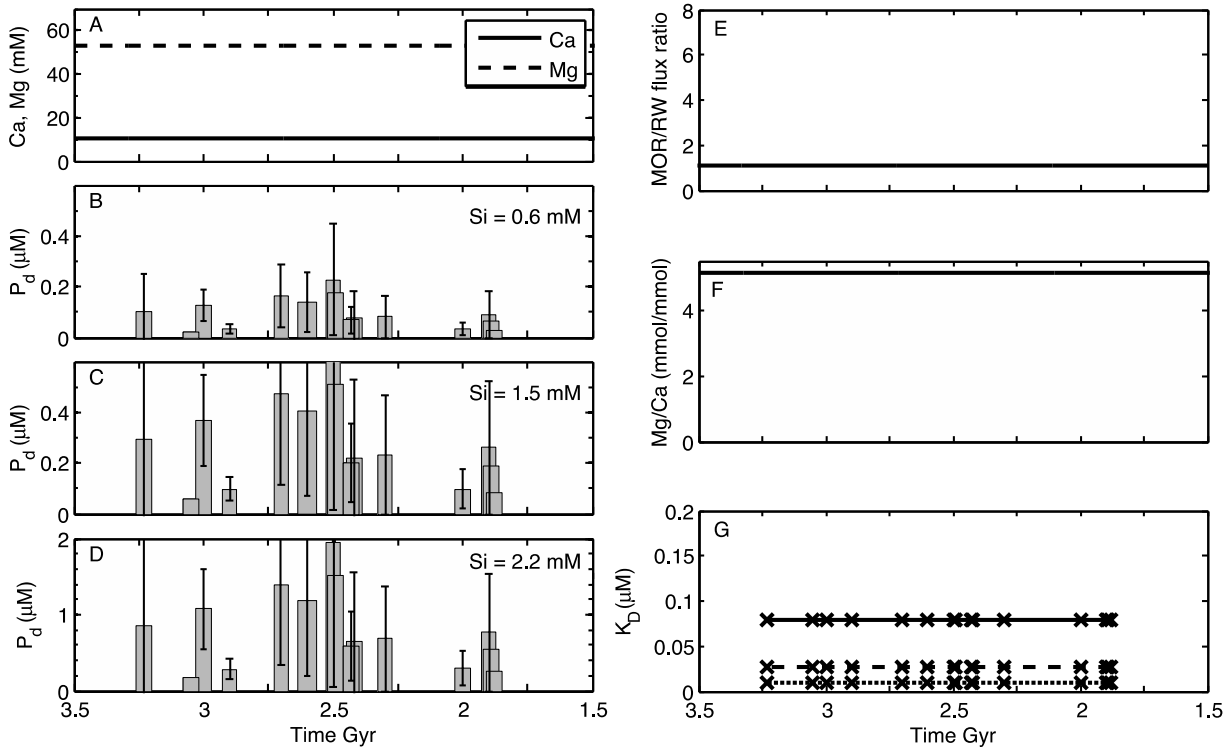

Figure DR6: The modern case of our model. Labels are as in Figure DR2.

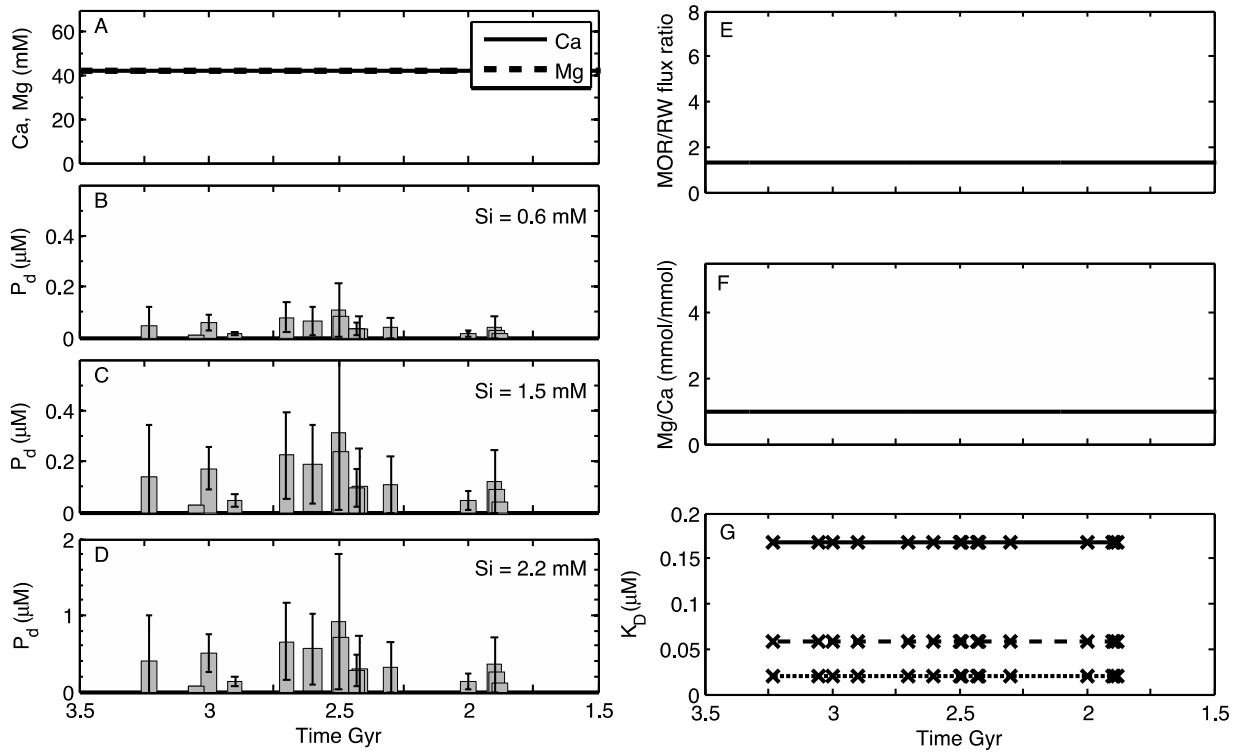

Figure DR7: The Cretaceous case of our model. Labels are as in Figure DR2.

While some parameters in our model have envelopes of uncertainty, our results from end member cases reveal little sensitivity in the resulting calculated P_d. In the extreme case using today's Mg and Ca concentrations, the estimated P_d would be roughly doubled relative to our base case. By far the largest uncertainty seems to be the degree of Si supersaturation of the Archean – early Proterozoic ocean.

We used the Si:Fe content of BIFs (Klein, 2005) to restrict the range of silica concentrations to those most likely in the Precambrian based on our silica sorption experiments (Fig. 2). These estimates are conservative given that 1) some iron may have been lost from the sediments during diagenesis, raising the Si:Fe and 2) any other source of silica precipitation not associated with Fe would also raise the observed Si:Fe.

Table DR1: Variables used to calculate dissolved phosphorus (P_d) from 3.5 to 1.5 Ga at varying silica concentrations in our base model.

Age	Modeled Ca (mM)	Modeled Mg (mM)	Si (mM)	K_D	P_d
-1.88	30.26	35.46	0.6	0.157	0.015
-1.89	28.84	38.83	0.6	0.150	0.034
-2	28.93	38.62	0.6	0.148	0.048
-1.9	28.51	39.63	0.6	0.151	0.018
-2.3	27.03	43.30	0.6	0.139	0.046
-2.42	34.72	25.34	0.6	0.173	0.035
-2.43	34.88	24.99	0.6	0.174	0.032
-2.49	37.56	19.24	0.6	0.179	0.078

-2.5	38.02	18.26	0.6	0.180	0.100
-2.6	39.07	16.04	0.6	0.182	0.061
-2.7	33.58	27.86	0.6	0.170	0.076
-2.9	34.41	26.03	0.6	0.172	0.015
-3.05	36.77	20.90	0.6	0.176	0.057
-3	35.98	22.60	0.6	0.178	0.009
-3.23	39.39	15.38	0.6	0.182	0.044
				mean	**0.044**

Age	Modeled Ca (mM)	Modeled Mg (mM)	Si (mM)	K_D	P_d
-1.88	30.26	35.46	1.5	0.055	0.042
-1.89	28.84	38.83	1.5	0.052	0.098
-2	28.93	38.62	1.5	0.051	0.138
-1.9	28.51	39.63	1.5	0.052	0.052
-2.3	27.03	43.30	1.5	0.048	0.132
-2.42	34.72	25.34	1.5	0.060	0.100
-2.43	34.88	24.99	1.5	0.060	0.091
-2.49	37.56	19.24	1.5	0.062	0.225
-2.5	38.02	18.26	1.5	0.062	0.288
-2.6	39.07	16.04	1.5	0.063	0.175
-2.7	33.58	27.86	1.5	0.059	0.220
-2.9	34.41	26.03	1.5	0.060	0.045
-3.05	36.77	20.90	1.5	0.061	0.164
-3	35.98	22.60	1.5	0.062	0.026
-3.23	39.39	15.38	1.5	0.063	0.127
				mean	**0.128**

Age	Modeled Ca (mM)	Modeled Mg (mM)	Si (mM)	K_D	P_d
-1.88	30.26	35.46	2.2	0.019	0.124
-1.89	28.84	38.83	2.2	0.018	0.288
-2	28.93	38.62	2.2	0.017	0.406
-1.9	28.51	39.63	2.2	0.018	0.152
-2.3	27.03	43.30	2.2	0.016	0.390
-2.42	34.72	25.34	2.2	0.020	0.294
-2.43	34.88	24.99	2.2	0.020	0.269
-2.49	37.56	19.24	2.2	0.021	0.663
-2.5	38.02	18.26	2.2	0.021	0.849
-2.6	39.07	16.04	2.2	0.021	0.514
-2.7	33.58	27.86	2.2	0.020	0.649
-2.9	34.41	26.03	2.2	0.020	0.132
-3.05	36.77	20.90	2.2	0.021	0.482
-3	35.98	22.60	2.2	0.021	0.075
-3.23	39.39	15.38	2.2	0.021	0.373
				mean	**0.375**

References

Bjerrum, C. J., and Canfield, D. E., 2004, New insights into the burial history of organic carbon on the early Earth: Geochemistry Geophysics Geosystems G3, v. 5, p. 10.1029/2004gc000713.

Condie, K. C., Belousova, E., Griffin, W. L., and Sircombe, K. N., 2009, Granitoid events in space and time: Constraints from igneous and detrital zircon age spectra: Gondwana Research, v. 15, no. 3-4, p. 228-242.

Fantle, M. S., and DePaolo, D. J., 2005, Variations in the marine Ca cycle over the past 20 million years: Earth and Planetary Science Letters, v. 237, no. 1-2, p. 102-117.

Grasshoff, K., Ehrhardt, M., and Kremling, K., 1999, Methods of seawater analysis, Weinheim Wiley-VCH, 600 p.:

Hardie, L. A., 2003, Secular variations in Precambrian seawater chemistry and the timing of Precambrian aragonite seas and calcite seas: Geology, v. 31, no. 9, p. 785-788.

Kamber, B. S., Greig, A., Schoenberg, R., and Collerson, K. D., 2003, A refined solution to Earth's hidden niobium: implications for evolution of continental crust and mode of core formation: Precambrian Research, v. 126, no. 3-4, p. 289-308.

Klein, C., 2005, Some Precambrian banded iron-formations (BIFs) from around the world: Their age, geologic setting, mineralogy, metamorphism, geochemistry, and origin: American Mineralogist, v. 90, no. 10, p. 1473-1499.

Korenaga, J., 2011, Thermal evolution with a hydrating mantle and the initiation of plate tectonics in the early Earth: Journal of Geophysical Research-Solid Earth, v. 116.

Sleep, N. H., and Zahnle, K., 2001, Carbon dioxide cycling and implications for climate on ancient Earth: Journal of Geophysical Research-Planets, v. 106, no. E1, p. 1373-1399.